This is the accepted manuscript made available via CHORUS. The article has been published as:

Numerical investigations of SO(4) emergent extended symmetry in spin-1/2 Heisenberg antiferromagnetic chains

Pranay Patil, Emanuel Katz, and Anders W. Sandvik

Phys. Rev. B **98**, 014414 — Published 10 July 2018

DOI: 10.1103/PhysRevB.98.014414

Numerical Investigations of SO(4) Emergent Extended Symmetry in Spin-1/2 Heisenberg Antiferromagnetic Chains

Pranay Patil,[1] Emanuel Katz,[1] and Anders W. Sandvik[1,2]

[1] *Department of Physics, Boston University, 590 Commonwealth Avenue, Boston, Massachusetts 02215, USA*
[2] *Beijing National Laboratory for Condensed Matter Physics and Institute of Physics, Chinese Academy of Sciences, Beijing 100190, China*

The antiferromagnetic Heisenberg chain is expected to have an extended symmetry, $[SU(2)\times SU(2)]/Z_2$, in the infrared limit, whose physical interpretation is that the spin and dimer order parameters form the components of a common 4-dimensional pseudovector. Here we numerically investigate this emergent symmetry using quantum Monte Carlo simulations of a modified Heisenberg chain (the J-Q model) in which the logarithmic scaling corrections of the conventional Heisenberg chain can be avoided. We show how the two- and three-point spin and dimer correlation functions approach their forms constrained by conformal field theory as the system size increases and numerically confirm the expected effects of the extended symmetry on various correlation functions. We stress that some times the leading power laws of three-point (and higher) correlations are not given simply by the scaling dimensions of the lattice operators involved, but can be faster decaying because of exact cancellations of contributions from the fields and currents under conformal symmetry.

I. INTRODUCTION

The development of the theory of deconfined quantum criticality [1] has reignited interest in critical quantum systems which show an extended symmetry in the thermodynamic limit [2–4]. An example of emergent symmetry can be seen in the spin-1/2 Heisenberg antiferromagnetic chain, where it is expected [5, 6] that the microscopic SU(2) symmetry extends to an $[SU(2)\times SU(2)]/Z_2$ symmetry. The ground state of this Hamiltonian is known to be critical and has been shown to have scale invariant behavior analytically [7] and numerically [8]. In this work, the emergence of the extended symmetry is connected to the behavior of two- and three-point correlation functions, thus providing a bridge between the continuum field theory and lattice correlation functions.

We will first connect the emergent symmetry to lattice correlation functions, then numerically study the correlations and show that they reflect the emergent symmetry. The correlation functions have strict functional forms which are controlled by the 2D conformal field theory (CFT) which describes the emergent physics. The emergent $[SU(2)\times SU(2)]/Z_2$ symmetry is manifested in the three components of the Néel order parameter and the dimer order parameter (which quantifies the spin-Peierls order) forming an SO(4) symmetric pseudovector [9]. The Z_2 reduction to the $SU(2)\times SU(2)$ is required as it is a "double cover" of SO(4) [10], i.e, there are two sets of SU(2) matrices which generate the same SO(4) rotation. The three-point functions of these order parameters can yield useful information about the emergent symmetry but must be treated with care, as a naive addition of scaling dimensions to infer the exponent of the power-law decay fails. An example of this will be presented here with the spin-spin-dimer three-point function in the Heisenberg chain. We discuss how the connections between the continuum and lattice version of the correlation functions have to be carefully considered in order to predict the correct power-law decay of the three-point function based on the CFT.

The outline of the paper is as follows: In Sec. II we review the predictions from renormalization group (RG) analysis and examine how the extended symmetry affects the correlation functions of the continuum versions of the lattice spin and dimer operators. In Sec. III, we present the manifestation of a CFT description on the correlation functions and benchmark these findings against numerical simulations of the transverse field Ising model (TFIM) on a periodic chain. We stitch together the results of these two sections in Sec. IV and predict the complete functional forms for the correlation functions and then present numerical evidence to support the same. We briefly summarize the study and discuss possible future applications of numerical CFT tests in Sec. V.

II. EMERGENCE OF $[SU(2)\times SU(2)]/Z_2$ SYMMETRY

The spin-1/2 Heisenberg chain, with the Hamiltonian

$$H = \sum_{i=1}^{N} \vec{\mathbb{S}}_i \cdot \vec{\mathbb{S}}_{i+1} \tag{1}$$

can be transformed into a system of interacting spinless fermions of two species using the transformation [5, 6]

$$\vec{\mathbb{S}}_n = \frac{1}{2}\psi^{\dagger}{}^{i}_{n}\vec{\boldsymbol{\sigma}}^{j}_{i}\psi_{nj}, \tag{2}$$

where ψ^i_n is a spin doublet and repeated indices imply summation over the range of values that the index can take (as we will use thoughout this work). To take the continuum limit, we will reiterate the series of arguments presented in [5, 6] and use this process to define quantities

that we will use later. Each fermion in the doublet can be rewritten as two new fermions,

$$\psi_n^j \simeq [i^n \psi_L^j (n \pm \frac{1}{2}) + (-i)^n \psi_R^j (n \pm \frac{1}{2})], \tag{3}$$

(plus and minus for even and odd n, respectively) which is an exact transformation up to an overall factor. This is motivated by the expectation that the free-fermion ground state would have all states with $|k| < \pi/2a$ occupied and then only Fourier modes with $k \simeq \pm\pi/2a$ would be important [11]. Thus, we understand the left (L) and right (R) fermion operators to be "locally" constant and to be slowly varying at the scale of lattice separation. These will ultimately form the operators of the continuum field theory. We can now write the spin operator on the lattice, using the current operators

$$\vec{J}_L = {\psi^\dagger}_L^i \vec{\boldsymbol{\sigma}}_i^j \psi_{Lj}, \tag{4a}$$

$$\vec{J}_R = {\psi^\dagger}_R^i \vec{\boldsymbol{\sigma}}_i^j \psi_{Rj}, \tag{4b}$$

and the fermion biliear

$$\boldsymbol{G}_j^i = {\psi^\dagger}_L^i \psi_{Rj}, \tag{5}$$

by direct substitution in Eq. (2) as

$$\mathbb{S}_n^i = a(J_L^i + J_R^i) + (-1)^n a \mathrm{Tr}[(\boldsymbol{G} - \boldsymbol{G}^\dagger)\boldsymbol{\sigma}^i]. \tag{6}$$

Here we have used script letters for lattice operators and bold font for matrices and we will continue to maintain these conventions throughout this text. The operators $\vec{J}_L, \vec{J}_R, \boldsymbol{G}$ are defined at the same lattice position n as the spin operator but this is not explicitly indicated to keep the equations unencumbered. This form of the spin operator can be substituted into the Hamiltonian of Eq. (1), which upon coarse graining has the following continuum limit,

$$H = (a/2) \int dx [\vec{J}_L \cdot \vec{J}_L + \vec{J}_R \cdot \vec{J}_R + 2\vec{J}_L \cdot \vec{J}_R] + ..., \tag{7}$$

where a is the lattice spacing [5].

Note also that at this stage we have only one SU(2) symmetry which comes along with the 3D rotation symmetry that the microscopic model has. This is manifest in each of $\vec{J}_{L/R}$ but they are not free to turn through different arbitrary angles due to the $\vec{J}_L \cdot \vec{J}_R$ term which keeps the relative angle between them fixed. Assuming that this Hamiltonian flows to the free fermion fixed point, which has the Hamiltonian

$$H_{fixed} = \int dx [\vec{J}_L \cdot \vec{J}_L + \vec{J}_R \cdot \vec{J}_R], \tag{8}$$

it can be shown that the term that couples left and right currents in Eq. (7) is irrelavant under RG flow [5, 6] for this particular fixed point. This is not true for all perturbations to the fixed point Hamiltonian and thus was checked explicitly [5, 6] for the $\vec{J}_L \cdot \vec{J}_R$ term. Thus we see that this line of reasoning leads us to believe that in the thermodynamic limit we should be left with the free fermion fixed point, which is also described by the $k = 1$ Wess-Zumino-Witten (WZW) conformal field theory [12].

To understand how the decoupling of the currents affects correlation functions of spin and dimer operators, we must first connect the primary operators of the CFT to these order parameters. Once we have done this, we can use the constraints that the extended symmetry places on the correlation functions of the primary operators to understand the correlations of the measurable orders.

The primary operators of the $k = 1$ WZW theory that we are going to be interested in are $[\boldsymbol{J_L}, \boldsymbol{J_R}, \boldsymbol{g}]$, which are the left and right currents with scaling dimension 1 and the primary field with scaling dimension 1/2. These are all SU(2) matrices, although the currents form matrices which belong to the Hermitian subset of SU(2), which are described by SO(3) vectors. This can be seen by observing that $\vec{J}_{L/R}$ in the fixed point Hamiltonian [Eq. (8)] are SO(3) vectors and thus the matrices to represent these must be written as

$$\boldsymbol{J_{L/R}} = J_{L/R}^a \boldsymbol{\sigma^a}, \tag{9}$$

where $J_{L/R}^a$ form the components of $\vec{J}_{L/R}$. This structure is also justified by the framework of the 2D CFT, which requires independent generators of translations for z and $\bar{z}$ (conjugate variables in the complex plane). In the Virasoro algebra of the 2D CFT [13], these would usually be called $J(z)$ and $\bar{J}(\bar{z})$ and in the case of the left (right) fermion, $z = x + it$ ($\bar{z} = x - it$) would encode its space-time position.

The primary field $\boldsymbol{g}$ is made out of the continuum versions of the lattice operators which we shall denote as (S^a, D). The components S^a form the continuum spin operators and D represents the continuum dimer operator. These together form an SO(4) pseudovector which is embedded in $\boldsymbol{g}$ through

$$\boldsymbol{g} = S^a \; i\boldsymbol{\sigma^a} + D\boldsymbol{I}, \tag{10}$$

as any general SU(2) matrix can be expanded in this manner. The continuum versions of spins and dimers will be mapped back to the lattice variables in the next section. The primary field $\boldsymbol{g}$ is also closely related to the fermion bilinear $\boldsymbol{G}$ as $\boldsymbol{g}$ is influenced by transformations in both z and $\bar{z}$ (left and right rotations) and $\boldsymbol{G}$ is made out of left- and right-moving fermions and is also sensitive to transformations in both of them.

As mentioned earlier, the left and right currents can turn through different arbitrary angles at the fixed point and these SO(3) rotations can be written in terms of transformations on the SU(2) matrices as

$$\boldsymbol{J_L} = J_L^a \boldsymbol{\sigma^a} \rightarrow \boldsymbol{L J_L L^\dagger} = J_L^{'a} \boldsymbol{\sigma^a}, \tag{11a}$$

$$\boldsymbol{J_R} = J_R^a \boldsymbol{\sigma^a} \rightarrow \boldsymbol{R J_R R^\dagger} = J_R^{'a} \boldsymbol{\sigma^a}, \tag{11b}$$

where $\boldsymbol{L}$ and $\boldsymbol{R}$ are the SU(2) rotation matrices. It is important to note here that these rotations do not mix left and right currents and keep the 2D conformal structure intact. The field $\boldsymbol{g}$ depends on z and $\bar{z}$ by construction [13] and thus is affected by both left and right rotations. These rotations are reflected in (S^a, D) through

$$\boldsymbol{g} = S^a \; i\boldsymbol{\sigma^a} + D\boldsymbol{I} \rightarrow \boldsymbol{L}\boldsymbol{g}\boldsymbol{R}^\dagger = S^{'a} \; i\boldsymbol{\sigma^a} + D^{'}\boldsymbol{I}, \quad (12)$$

which creates the new set $(S^{'a}, D^{'})$. The matrices $(\boldsymbol{g}, \boldsymbol{J_L}, \boldsymbol{J_R})$ live on the complex plane formed by spacetime and so do their components. The correlation functions of these components (which are the continuum spin, dimer, and current operators) on the complex plane are of interest to us as they tell us what to expect for the correlation functions of the lattice operators, which we will investigate numerically later. We would also like to point out here that all the correlation functions that we consider in this text are connected correlation functions as they are the ones which the CFT predicts. From this point on, we will not explicitly mention that we are only considering connected correlation functions. For the continuum operators, the connected correlation functions we consider are the same as the naive correlation functions as all the operators have a zero single body expectation (enforced by the CFT) value and this implies nothing needs to be subtracted from the naive correlation function to get the connected one.

To extract the correlation functions of (S^a, D), we examine

$$\langle \mathrm{Tr}[\boldsymbol{g}_{z_1}\boldsymbol{g}^\dagger_{z_2}]\rangle = \langle S^a S^a\rangle + \langle DD\rangle \quad (13)$$

and see that the right hand side is non-zero as the arbitrary transformations $\boldsymbol{L}$ and $\boldsymbol{R}$ leave the two point function of $\boldsymbol{g}$, as defined here, unchanged through Eq. (12) due to the cyclicity of the trace and as $\boldsymbol{R}^\dagger\boldsymbol{R} = \boldsymbol{L}^\dagger\boldsymbol{L} = \boldsymbol{I}$. Similarly, if we look at the transformation of the three-point function,

$$\begin{aligned}&\langle \mathrm{Tr}[\boldsymbol{g}_{\boldsymbol{z_1}}\boldsymbol{g}^\dagger_{z_2}\boldsymbol{g}_{\boldsymbol{z_3}}]\rangle \rightarrow \quad (14)\\ &\quad \langle \mathrm{Tr}[\boldsymbol{L}\boldsymbol{g}_{z_1}\boldsymbol{R}^\dagger\boldsymbol{R}\boldsymbol{g}^\dagger{}_{z_2}\boldsymbol{L}^\dagger\boldsymbol{L}\boldsymbol{g}_{z_3}\boldsymbol{R}^\dagger]\rangle,\end{aligned}$$

we see that the only way to keep this invariant under arbitrary $\boldsymbol{L}$ and $\boldsymbol{R}$ would be to have this vanish. The vanishing of the three-point function then implies that all three-point functions of (S^a, D) (which could be either of $\langle S^a S^a D\rangle, \langle S^a D S^a\rangle, \langle D S^a S^a\rangle, \langle DDD\rangle$) would vanish. This can be seen by writing down all the possible three-point functions of $\boldsymbol{g}$ and $\boldsymbol{g}^\dagger$ and solving for the spin and dimer correlation functions.

When discussing the lattice spin and dimer correlation functions, we will also need the continuum versions of the correlation functions of the currents and operators. The expressions which are of interest to us and robust against arbitrary $\boldsymbol{L}$ and $\boldsymbol{R}$ transformations are

$$\langle \mathrm{Tr}[\boldsymbol{J_L}\boldsymbol{J_L}]\rangle \sim \langle J^a_L J^a_L\rangle, \quad (15)$$

$$\langle \mathrm{Tr}[\boldsymbol{J_L}\boldsymbol{g}\boldsymbol{g}^\dagger]\rangle \sim \langle J^a_L S^a D\rangle + \langle J^a_L D S^a\rangle, \quad (16)$$

and permutations of the second equation with $\boldsymbol{J_L}$ in different positions. These equations also apply for the right currents by just switching all $L \rightarrow R$. The non-vanishing nature of these correlation functions can be seen again using the cyclicity of the trace and transformation equations (11a), (11b) and (12).

III. CFT AND CORRELATION FUNCTIONS

Due to the mapping to massless fermions, the spin-1/2 Heisenberg chain is a 2D CFT and we can use the constraints the 2D CFT puts on the correlation functions to understand their precise forms. A 2D CFT is defined on the complex plane and the constraints that conformal symmetry requires restricts the two and three-point correlation functions of primary operators to behave as [13]

$$\langle O_i O_j\rangle \sim \frac{\delta_{ij}}{|z_{ij}|^{\Lambda_i\Lambda_j}}, \quad (17a)$$

$$\langle O_i O_j O_k\rangle \sim \frac{1}{|z_{ij}|^{\Delta_{ij}}|z_{jk}|^{\Delta_{jk}}|z_{ki}|^{\Delta_{ki}}}, \quad (17b)$$

where O_i are the primary operators of the CFT and Λ_i are their scaling dimensions and $\Delta_{ij} = \Lambda_i + \Lambda_j - \Lambda_k$. The scaling dimension of a primary operator is made up of two numbers h_i and $\bar{h}_i$ which indicate the scaling in z and $\bar{z}$ respectively. These correlation functions can be factorised into two pieces, where one depends on z, and the other on $\bar{z}$ and the Λ_i's are replaced by $h_i(\bar{h}_i)$. This is useful when $h_i \neq \bar{h}_i$, which may be the case for current operators, which generate translations in either z or $\bar{z}$. For operators with $h_i = \bar{h}_i$, we do not mention each of them separately, but only indicate the total scaling dimension $\Lambda_i = h_i + \bar{h}_i$.

As these relations are valid on the infinite complex plane and our simulations are done on a periodic chain, we must use a mapping from the cylinder to the infinite plane to understand the correlation functions. In our simulations, we use ground state projector quantum Monte Carlo (QMC) simulations, which means that we project on a trial state with a large number of Hamiltonians, effectively for a long imaginary time. This implies that we are using a cylinder whose circumference is the system size and length is infinite for all practical purposes. The system can then be mapped to the infinite plane through the transformations $\tau \rightarrow r$ and $x \rightarrow \theta$ [14] which results in two spatially separated points on the periodic chain having a conformal distance between them of

$$|z_{ij}| = L \sin\left(\pi\frac{x}{L}\right), \quad (18)$$

where x is the separation on the ring. This substitution into the correlation functions on the plane tells us what we should expect on the cylinder. In some cases,

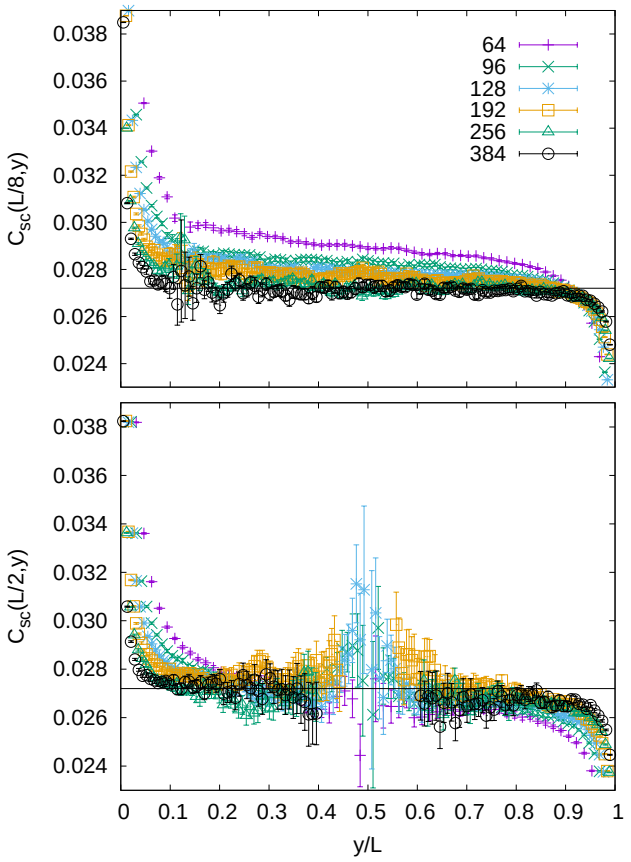

FIG. 1. The scaled three-point function for the critical periodic TFIM chain as defined in Eq. (21) flows to a constant for $x = L/8$ and $x = L/2$. The line is a guide to the eye and for $x = L/2$, we only exclude data around $y/L = 0.5$ for large sizes as the correlation function vanishes quickly as $x \sim y \sim L/2$ and this means the numerical signal is very weak.

the correlation function on the plane may have different dependence on z and $\bar{z}$ and may not be expressible in $|z|$, but the mapping to the cylinder correlation functions reverses this [13, 14] and they only depend on the conformal distance given by Eq. (18), which must be the case as they are real. Conformal information has also been used to aid fitting of correlation functions and other numerical quantities for spin systems [15–17]. The conformal structure of Potts models has also been investigated using three-point functions[18]. As we will see, the SU(2) spin chains considered here have additional complications when interpreting multi-point functions.

As a warm-up, we first consider the much simpler case of the TFIM chain, whose two-point function was already analyzed alongside that of SU(2) chains in Ref. 19. Its Hamiltonian is

$$H = -\sum_{i=1}^{N} \sigma_i^z \sigma_{i+1}^z - \sum_{i=1}^{N} \sigma_i^x. \tag{19}$$

Here we will check that the functional form of the three-point function matches the CFT prediction for the TFIM as we will be using three-point functions in the next section to point out features of the extended symmetry. The CFT of the TFIM is made up of three primary operators, namely the identity I, the spin σ and the ferromagnetic part of the energy density ϵ, with scaling dimensions 0, 1/8 and 1 respectively [12, 20]. With these operators, the non-vanishing three-point function with the smallest scaling dimension is $\langle \epsilon\sigma\sigma \rangle$. We also note here again that the CFT only tells us the behavior of the connected three-point function and due to this, we compare the CFT expectation to $\langle \epsilon\sigma\sigma \rangle_c = \langle \epsilon\sigma\sigma \rangle - \langle \epsilon \rangle \langle \sigma\sigma \rangle$. We will not carry the subscript c for connected correlation functions as they make the symbolic expressions cumbersome.

Using the conformal distance and Eq. (17b), the three-point correlation function on the ring should be

$$\langle \epsilon_0 \sigma_x \sigma_y \rangle \sim \frac{\left[L \sin\left(\pi \frac{|y-x|}{L}\right)\right]^{\frac{3}{4}}}{\left[L \sin\left(\pi \frac{x}{L}\right)\right]\left[L \sin\left(\pi \frac{y}{L}\right)\right]}. \tag{20}$$

To compare numerical data to this expression, we define a scaled correlation function $C_{sc}(x, y)$ which is the raw correlation function multiplied by the inverse of the expected form as shown below:

$$C_{sc}(x, y) \sim \langle \epsilon_0 \sigma_x \sigma_y \rangle \times \frac{\left[L \sin\left(\pi \frac{x}{L}\right)\right]\left[L \sin\left(\pi \frac{y}{L}\right)\right]}{\left[L \sin\left(\pi \frac{|y-x|}{L}\right)\right]^{\frac{3}{4}}} \tag{21}$$

If the expression matches, we should expect the scaled correlation function to be a constant as a function of x and y. In Fig. 1, we plot the scaled correlation function for two different values of x and the whole range of y. For large sizes, we observe an approach to constant behavior, with the deviations occurring when two out of the three operators are close to each other and, therefore, the coarse grained description does not hold.

It is important to note here that we must use the conformal distances when predicting the finite-size functional form due to the cylinder to plane conformal transformation that we have used. We can also define the scaled correlation function using just the lattice distances instead of the conformal distance as

$$C_{sc}(x, y) \sim \langle \epsilon_0 \sigma_x \sigma_y \rangle \times \frac{[s(0, x)][s(0, y)]}{[s(x, y)]^{\frac{3}{4}}}, \tag{22}$$

where $s(a, b)$ is the shortest distance between a and b along the ring. This way of defining the scaled correlator results in a disagreement with the expected constant form for the scaled correlation function, as can be seen in Fig. 2, although the curves for different sizes still show data collapse as the correct scaling dimension is being used even in this correlator. The above manner of using scaled correlation functions such as Eq. (21) has already been used in previous work [19] for the two-point spin correlation function, and will also be used in the next section to test the agreement to the predictions of Sec. II.

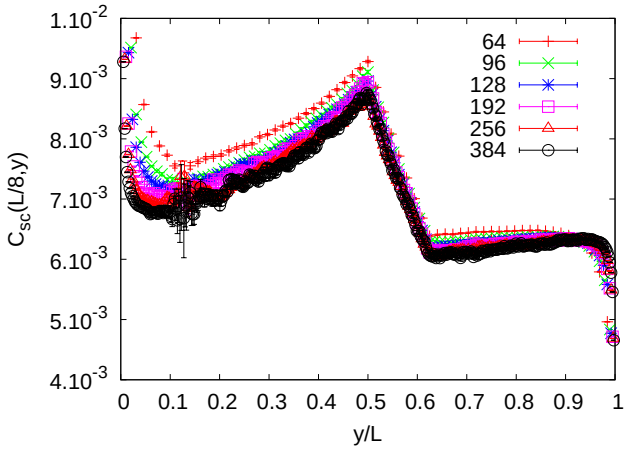

FIG. 2. Three point function for the critical TFIM periodic chain scaled using the lattice distance rather than the conformal distance, here for $x = L/8$.

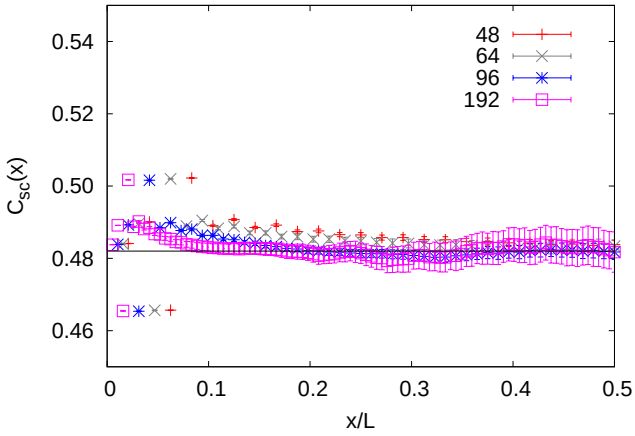

FIG. 3. Scaled dimer two-point function for the critical JQ_2 periodic chain as defined in Eq. (31). The results flow to a constant with increasing size. The Horizontal axis only extends to $x/L = 0.5$ as two-point functions are symmetric about $y = L/2$.

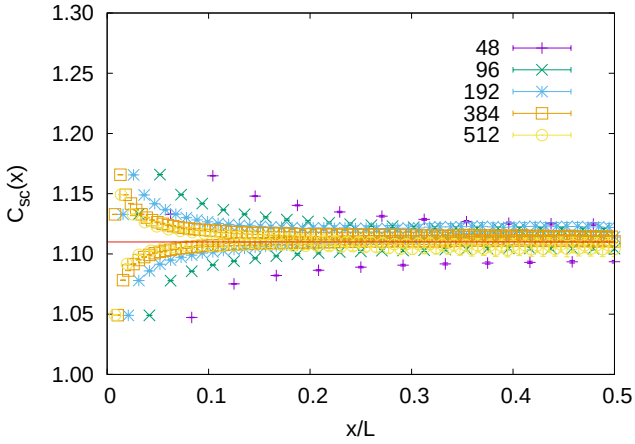

FIG. 4. Spin two-point function for the critical JQ_2 chain scaled with the first term of Eq. (28) [as explicitly shown in Eq. (32)]. The approach to a constant for large sizes confirms the expected form.

IV. LATTICE CORRELATION FUNCTION NUMERICS

In Sec. II, we have seen that some of the correlation functions of continuum operators vanish and for the ones that do not, we can predict their functional forms based on the CFT constraints presented in Sec. III. The primary operators of the $k = 1$ WZW model are $\boldsymbol{J_L}, \boldsymbol{J_R}$ and $\boldsymbol{g}$ with scaling dimensions $(h, \bar{h})$ given by (1,0),(0,1) and (1/4,1/4) respectively. Using these dimensions, we can infer that the correlation functions on the periodic chain must have the following forms,

$$\langle \mathrm{Tr}[\boldsymbol{g}(0)\boldsymbol{g}^\dagger(x)]\rangle \sim \frac{1}{L\sin(\pi\frac{x}{L})}, \tag{23a}$$

$$\langle \mathrm{Tr}[\boldsymbol{J_L}(0)\boldsymbol{J_L}(x)]\rangle \sim \frac{1}{\left[L\sin(\pi\frac{x}{L})\right]^2}, \tag{23b}$$

$$\langle \mathrm{Tr}[\boldsymbol{J_L}(0)\boldsymbol{g}(x)\boldsymbol{g}^\dagger(y)]\rangle \sim \frac{1}{\left[L\sin(\pi\frac{x}{L})\right]\left[L\sin(\pi\frac{y}{L})\right]}, \tag{23c}$$

and the same for $L \to R$. We can now use these expressions to understand the lattice correlation functions by writing the lattice operators in terms of their continuum versions. Inspired by the analysis leading upto Eq. (6), the spin and dimer lattice operators have been postulated [5, 9] to be

$$\mathbb{S}^i_n \sim \alpha(J^i_L + J^i_R) + (-1)^n\beta S^i, \tag{24a}$$

$$\mathbb{D}_n = \vec{\mathbb{S}}_n \cdot \vec{\mathbb{S}}_{n+1} \sim D_0 + (-1)^n\gamma D, \tag{24b}$$

where α, β, γ are UV sensitive prefactors and D_0 is a constant shift of the lattice dimer operator which must be subtracted out when calculating connected correlation functions.

Using this equivalence between the lattice and continuum operators, we can construct the lattice correlation functions that we are going to use;

$$\langle \mathbb{D}\mathbb{D}\rangle \sim (-1)^n\langle Tr[\boldsymbol{g}\boldsymbol{g}^\dagger]\rangle + ..., \tag{25a}$$

$$\langle \mathbb{D}\mathbb{D}\mathbb{D}\rangle \sim 0 + ..., \tag{25b}$$

$$\langle \vec{\mathbb{S}}\cdot\vec{\mathbb{S}}\rangle \sim (-1)^n\langle Tr[\boldsymbol{g}\boldsymbol{g}^\dagger]\rangle + \langle \vec{J}_L\cdot\vec{J}_L\rangle + \langle \vec{J}_R\cdot\vec{J}_R\rangle + ..., \tag{25c}$$

$$\langle \vec{\mathbb{S}}\cdot\vec{\mathbb{D}}\rangle \sim \langle Tr[\boldsymbol{J_L}\boldsymbol{g}\boldsymbol{g}^\dagger]\rangle + \langle Tr[\boldsymbol{g}\boldsymbol{J_L}\boldsymbol{g}^\dagger]\rangle + (L \to R) + ..., \tag{25d}$$

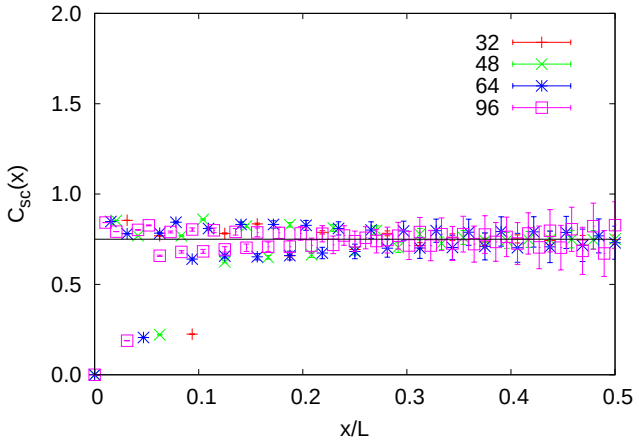

FIG. 5. Spin two-point function for the critical JQ_2 chain with the first term of Eq. (28) subtracted out and scaled with the second term, as in Eq. (33). We see improving agreement with the expected form with increasing L.

where we have dropped the prefactors as they are UV-controlled parameters which are not important from the continuum perspective and to keep the equations from becoming unnecessarily dense. The additional terms ignored in these equations are lattice non-asymptotic corrections which occur due to finite distance and lattice size. Our simulations use lattices large enough to observe the decay toward zero of these contributions.

We can incorporate the results of Eqs. (23a), (23b) and (23c) to hypothesize that the full functional forms of the connected lattice correlation functions are

$$\langle \mathbb{D}_0 \mathbb{D}_x \mathbb{D}_y \rangle \sim 0 + ..., \tag{26}$$

$$\langle \mathbb{D}_0 \mathbb{D}_x \rangle \sim \frac{(-1)^x}{L \sin(\pi \frac{x}{L})} + ..., \tag{27}$$

$$\langle \vec{\mathbb{S}}_0 \cdot \vec{\mathbb{S}}_x \rangle \sim \frac{(-1)^x}{L \sin(\pi \frac{x}{L})} + \frac{1}{\left[L \sin(\pi \frac{x}{L})\right]^2} + ..., \tag{28}$$

$$\langle \mathbb{D}_0 \vec{\mathbb{S}}_x \cdot \vec{\mathbb{S}}_y \rangle \sim \frac{1}{L \sin\left[\frac{\pi}{L}(y-x)\right]} \left[\frac{(-1)^x}{L \sin(\pi \frac{y}{L})} - \frac{(-1)^y}{L \sin(\pi \frac{x}{L})} \right] + ... \tag{29}$$

The most striking effects of the extended symmetry are seen in Eqs. (26) and (29) where the vanishing of the three-point function of $\boldsymbol{g}$ ensures that there is no term with scaling dimension 3/2 (three times scaling dimension of $\boldsymbol{g}$) in either of these equations. In this case, if we were to use the three-point function's scaling form to infer the scaling dimensions of the operators (which imply the scaling dimensions should sum to 2), we would run into errors as we would be unable to make it consistent with the two point functions (which imply the scaling dimensions should sum to 3/2). To see proof of this

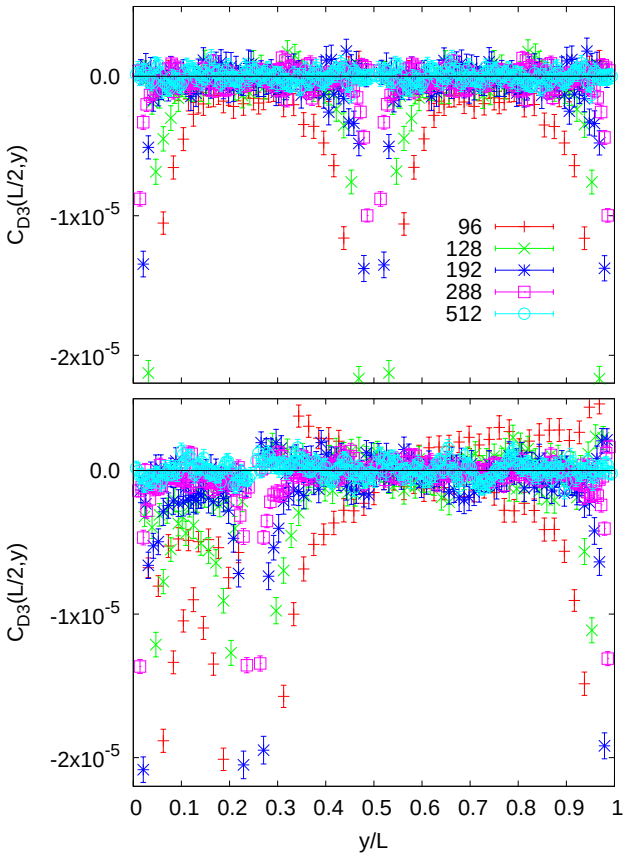

FIG. 6. The Dimer three-point function for the critical JQ_2 chain vanishes for large enough system size, which agreement with Eq. (26), here shown for $x = L/4$ and $x = L/2$.

numerically, we again calculate scaled correlation functions for these expressions, except for $\langle \mathbb{D}_0 \mathbb{D}_x \mathbb{D}_y \rangle$, which is expected to be zero. If the numerics agree, we should expect to see that the scaled functions are constants with respect to x and y, as seen in Sec. III for the TFIM.

The continuum description of the Heisenberg model ground state has marginal operators which lead to log corrections to correlation functions. We shall use the JQ_2 chain which is the Heisenberg model with a four spin term that enforces dimer order when strong and tunes out the log corrections at the transition point (where the marginal operator vanishes) into the dimer phase;

$$H = -J \Sigma_i \mathbb{P}_{i,i+1} - Q \Sigma_i \mathbb{P}_{i,i+1} \mathbb{P}_{i+2,i+3} \tag{30}$$

where $\mathbb{P}_{i,j} = 1/4 - \vec{\mathbb{S}}_i \cdot \vec{\mathbb{S}}_j$. This model is an alternative to the more commonly used J_1-J_2 (first and second neighbor interacting) Heisenberg chain [21], with the advantage that it is amenable to QMC studies without sign problems.

At a critical value of Q/J, $Q_c/J \approx 0.84831$ [22, 23], we would expect to see the correlation functions behave according to the predicted forms. All our simulations of the ground state of the critical JQ_2 chain are done using

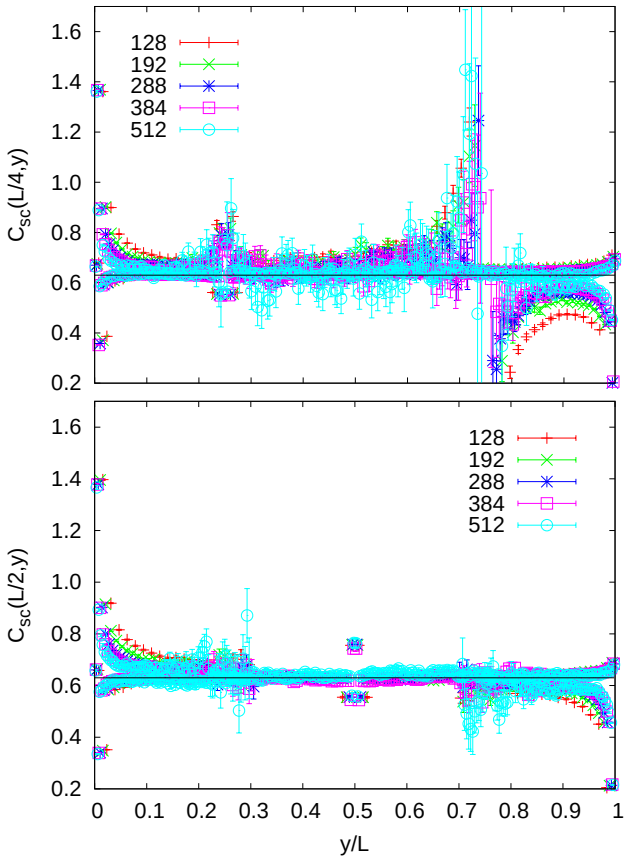

FIG. 7. The scaled dimer-spin-spin three-point function, Eq. (34), for the critical JQ_2 flows to a constant, here demonstrated for $x = L/4$ and $x = L/2$. In the upper panel, the divergence at $y = 3L/4$ is due to the exact vanishing of the correlation function at this point. In the lower panel, data for even y values in the range $y/L \in (0.3, 0.7)$ have been excluded as $\langle \mathbb{D}_0 \vec{\mathbb{S}}_x \cdot \vec{\mathbb{S}}_y \rangle$ tends to a "0/0" form and, thus, the scaled correlation function is very noisy.

a projector QMC method formulated in the valence-bond basis. The correlation functions are evaluated using loop estimators on the transition-graphs created by sampling the states in the valence-bond basis [24, 25]. Fig. 3 illustrates the scaled correlator for $\langle \mathbb{D}_0 \mathbb{D}_x \rangle$, defined using Eq. (27) as

$$C_{sc}(x) = \langle \mathbb{D}_0 \mathbb{D}_x \rangle \times \frac{L \sin(\pi \frac{x}{L})}{(-1)^x}, \tag{31}$$

and we see that it approaches a constant for fairly small chain lengths. Fig. 4 shows the scaled version of the first term (scaling dimension of 1) of $\langle \vec{\mathbb{S}}_0 \cdot \vec{\mathbb{S}}_x \rangle$, again defined using Eq. (28) as

$$C_{sc}(x) = \langle \vec{\mathbb{S}}_0 \cdot \vec{\mathbb{S}}_x \rangle \times \left[\frac{L \sin(\pi \frac{x}{L})}{(-1)^x} \right], \tag{32}$$

which dominates the second term (scaling dimension of 2) and we see that this flows to a constant [1.11(1)] with increasing size. In Fig. 5, we subtract out the first term and present the scaled version of the second term in a scaled correlation function defined as

$$C_{sc}(x) = \left[\langle \vec{\mathbb{S}}_0 \cdot \vec{\mathbb{S}}_x \rangle - 1.11 \times \frac{(-1)^x}{L \sin(\pi \frac{x}{L})} \right] \times \left[L \sin\left(\pi \frac{x}{L} \right) \right], \tag{33}$$

for which we cannot go to large sizes due to insufficient data quality. We still can observe that it matches our expectations, flowing to a constant with increasing system size.

In Fig. 6, we show the agreement of the three-point dimer correlation function [denoted by $C_{D3}(x, y)$ in both figures] with Eq. (26) for two different values of x and the whole range of y values. Only in the case of the three-point dimer function, we present the raw correlation function without scaling as it is expected to be zero and there is no sense in which we can scale it. We show the same for Eq. (29) through Figs. 7 by again defining a scaled correlator as

$$C_{sc}(x, y) = \langle \mathbb{D}_0 \vec{\mathbb{S}}_x \cdot \vec{\mathbb{S}}_y \rangle \frac{L \sin\left[\frac{\pi}{L}(y - x)\right]}{\frac{(-1)^x}{L \sin(\pi \frac{y}{L})} - \frac{(-1)^y}{L \sin(\pi \frac{x}{L})}} \tag{34}$$

and observing that it approaches a constant for large sizes. With this numerical evidence, we conclude that the signatures of the extended symmetry that we expect to see are indeed present in the spin-1/2 Heisenberg chain. Finite-size (distance) corrections can be seen clearly in our numerical data and these should be described by irrelevant operators.

V. CONCLUSION

We have shown numerical evidence of the effects of the emergent SO(4) $\equiv$ [SU(2)$\times$ SU(2)]/Z_2 symmetry in the Heisenberg chain on the correlation functions of lattice operators. This establishes the IR emergent symmetry which was theoretically expected from a variety of arguments. The three-point function was discussed here as a useful tool to understand the structure of the underlying field theory and has been shown to yield useful information through not only its scaling dimension, but also its functional form. The clearest example of this is $\langle \mathbb{D}_0 \vec{\mathbb{S}}_x \cdot \vec{\mathbb{S}}_y \rangle$ whose observed scaling dimension is not directly related to the leading scaling dimensions of the operators it is made out of, due to cancelations of contributions from the field and current operators. Here, we have also developed tests of CFT through correlation functions and these can be used to test suspected extended symmetry in higher dimensional systems[2, 3] and more broadly to test for CFT signatures in general.

In higher dimensions, an open question is what system geometry is best suited for investigating the conformal symmetry explicitly in equal-time correlation functions.

In 1D, for the ring geometry (infinite imaginary time, i.e., the ground state) the conformal distance naturally emerges, but it does not have a direct generalization to 2D or 3D. The functional form of the correlation functions when expressed using the conformal distance in 1D provides perhaps the most striking evidence of conformal invariance in finite systems, and such a concept in higher dimensions would be very useful for lattice calculations. QMC calculations of correlation functions can be readily extended to higher dimensions to check the existence of CFT descriptions if such concepts were to be developed. For 1D systems, density matrix renormalization group (DMRG) can be used to check the predictions of the CFT as well, including direct detection of the conformal tower of excitations [26]. With DMRG calculations using the common open boundary conditions (as the computational cost of periodic boundaries is significantly higher), CFT results for correlation functions will only be valid away from the boundaries, and the correlation functions will then just depend on the lattice separation between sites instead of the conformal distance (acheived by the mapping of the infinite cylinder to the infinite plane). This would be relevant when simulating the critical J_1-J_2 chain which is not amenable to QMC due to the sign problem but has the same CFT description as the J-Q chain considered here, and is another model which recreates the $k = 1$ WZW model in the continuum limit.

ACKNOWLEDGMENTS

We would like to thank Cenke Xu for useful discussions. AWS was supported by the NSF under Grant No. DMR-1710170 and by a Simons Investigator Grant. PP would like to thank the Institute of Physics, Chinese Academy of Sciences, for visitor support. The computational work was performed using the Shared Computing Cluster administered by Boston University's Research Computing Services. We used QuSpin for checking the Quantum Monte Carlo simulation against exact diagonalization calculations[27].

[1] T. Senthil, A. Vishwanath, L. Balents, S. Sachdev and M. P. A. Fisher, Science **303**, 1490 (2004).
[2] A. Nahum, P. Serna, J. T. Chalker, M. Ortuno and A. M. Somoza, Phys. Rev. Lett. **115**, 267203 (2015).
[3] C. Wang, A. Nahum, M. A. Metlitski, C. Xu and T. Senthil, Phys. Rev. X **7**, 031051 (2017).
[4] Y. Q. Qin, Y. -Y. He, Y. -Z. You, Z. -Y. Lu, A. Sen, A. W. Sandvik, C. Xu, and Z. Y. Meng, Phys. Rev. X **7**, 031052 (2017).
[5] I. Affleck, Phys. Rev. Lett. **55**, 1355 (1985).
[6] I. Affleck and F. D. M. Haldane, Phys. Rev. B **36**, 5291 (1987).
[7] T. Giamarchi and H. J. Schulz, Phys. Rev. B **39**, 4620 (1989).
[8] O. A. Starykh, R. R. P. Singh, and A. W. Sandvik, Phys. Rev. Lett. **78**, 539 (1997).
[9] A. M. Tsvelik, Cambridge University Press (2007).
[10] R. W. Carter, I. G. MacDonald, G. B. Segal, and M. Taylor, Cambridge University Press (1995).
[11] F. D. M. Haldane, Phys. Rev. Lett. **45**, 1358 (1980).
[12] A. A. Belavin, A. M. Polyakov and A. B. Zamolodchikov, Nucl. Phys. B **241**, 333 (1984).
[13] P. Francesco, P. Mathieu, and D. Sénéchal, Springer Science & Business Media (1997).
[14] P. Calabrese, and J. Cardy, J. Phys. A **42**, 504005 (2009).
[15] G. Fáth, Phys. Rev. B **68**, 134445 (2003).
[16] C. Arita and K. Motegi, J. Math. Phys. **52**, 063303 (2011).
[17] B. Lake, D. A. Tennannt, C. D. Frost and S. E. Nagler, Nature Mat. **4** 329 (2005).
[18] G. Delfino, M. Picco, R. Santachiara and J. Viti, J. Stat. Mech. P11011 (2013).
[19] P. Patil, Y. Tang, E. Katz, and A. W. Sandvik, Phys. Rev. B **96**, 045140 (2017).
[20] V. G. Knizhnik and A. B. Zamolodchikov, Nucl. Phys. B **247**, 83 (1984).
[21] S. Eggert, Phys. Rev. B **54**, R9612 (1996).
[22] Y. Tang and A. W. Sandvik, Phys. Rev. Lett. **107**, 157201 (2011).
[23] S. Sanyal, A. Banerjee, and K. Damle, Phys. Rev. B **84**, 235129 (2011).
[24] K. S. D. Beach and A. W. Sandvik, Nucl. Phys. B **750**, 142 (2006).
[25] A. W. Sandvik, and H. G. Evertz, Phys. Rev. B **82**, 024407 (2010).
[26] N. Chepiga and F. Mila, Phys. Rev. B **96**, 054425 (2017).
[27] P. Weinberg and M. Bukov, SciPost Phys. **2**, 003 (2017).